

Ultrahigh surface sensitivity of deposited gold nanorod arrays for nanoplasmonic biosensing

Abdul Rahim Ferhan^a, Youngkyu Hwang^{a,b}, Mohammed Shahrudin Bin Ibrahim^a, Shikhar Anand^{b,c}, Ahram Kim^{d,e}, Joshua A. Jackman^{b,*}, Nam-Joon Cho^{a,*}

^a School of Materials Science and Engineering, Nanyang Technological University, Singapore 639798, Singapore

^b School of Chemical Engineering and Biomedical Institute for Convergence at SKKU (BICS), Sungkyunkwan University, Suwon 16419, Republic of Korea

^c Department of Chemical Engineering, Indian Institute of Technology Delhi, New Delhi 110016, India

^d Omni Colab Corporation, Suwon 16229, Republic of Korea

^e LTIS Corporation, Suwon 16229, Republic of Korea

ARTICLE INFO

Article history:

Received 7 March 2021

Revised 31 March 2021

Accepted 15 April 2021

Keywords:

Nanoplasmonics

Localized surface plasmon resonance

Label-free biosensing

Surface sensitivity

Gold nanorods

ABSTRACT

The biosensing performance of plasmonic nanostructures critically depends on detecting changes in the local refractive index near the sensor surface, which is referred to as surface sensitivity. For biosensing applications at solid-liquid interfaces, recent efforts to boost surface sensitivity have narrowly focused on laterally isotropic nanostructures, while there is an outstanding need to explore laterally anisotropic nanostructures such as nanorods that have distinct plasmonic properties. Herein, we report the development of plasmonic gold nanorod (AuNR) arrays that exhibit ultrahigh surface sensitivity to detect various classes of biomacromolecular interactions with superior biosensing performance. A colloidal deposition strategy was devised to fabricate AuNR-coated glass substrates, along with experimental measurements and analytical calculations to investigate how nanorod dimensions and local dielectric environment affect plasmonic properties. To validate the sensing concept, real-time biosensing experiments involving protein adsorption and peptide-induced vesicle rupture were conducted and revealed that rationally tuning nanorod dimensions could yield AuNR arrays with the highest reported degree of surface sensitivity compared to a wide range of plasmonic nanostructures tested in past studies. We discuss plasmonic factors that contribute to this ultrahigh surface sensitivity and the measurement capabilities developed in this study are broadly extendable to a wide range of biosensing applications.

© 2021 Published by Elsevier Ltd.

1. Introduction

Nanoplasmonic sensors offer unparalleled measurement capabilities for tracking biomacromolecular interactions at solid-liquid interfaces on account of high measurement sensitivity, simple instrumental requirements, and label-free readout [1–5]. As the nanoplasmonic sensing field evolves from molecular detection to more advanced biosensing applications [6–11], there is strong interest in defining suitable performance metrics to guide sensor development based on a fundamental understanding of the plasmonic behavior [12–14].

When incident light interacts with metallic nanostructures, light extinction caused by absorption and/or scattering can induce the collective oscillation of conduction-band electrons in the metallic nanostructure, which results in a plasmon-enhanced elec-

tromagnetic field that is tightly confined to the sensor surface [1,15,16]. The decay length of this field enhancement effect is typically on the order of 5–20 nm [17,18] and biomacromolecular interaction events, such as adsorption and/or conformational changes, that occur within this probing volume will cause changes in the oscillation behavior. For metallic nanoparticles, the corresponding plasmonic phenomenon is called localized surface plasmon resonance (LSPR) whereby light extinction occurs across the UV-visible wavelength range, with a maximum at a particular wavelength λ_{\max} for each plasmon mode [15]. In LSPR measurements, if a biomacromolecular interaction occurs near the sensor surface, then there will be a change in the local refractive index that is typically reported in terms of $\Delta\lambda_{\max}$ shifts [3]. Accordingly, for biosensing applications, it is desirable to design nanoplasmonic sensors that elicit larger $\Delta\lambda_{\max}$ shifts for target biomacromolecular interactions, which can improve detection sensitivity, selectivity, and reliability [19–22]. Possible design strategies include selecting plasmonic nanostructures with larger field enhancements

* Corresponding authors.

E-mail addresses: jjackman@skku.edu (J.A. Jackman), njcho@ntu.edu.sg (N.-J. Cho).

(i.e., greater change in oscillation behavior) and/or shorter decay lengths (i.e., more occupied probing volume), while it is important to rationally tune the nanostructure design based on suitable performance criteria [9,14,23–27].

The main criteria to evaluate nanoplasmonic sensor performance has been the bulk refractive index sensitivity, which describes the measurement response to changes in the refractive index of the bulk solution above the sensor surface [24,28]. This evaluation approach was adapted from early efforts with conventional surface plasmon resonance (SPR) biosensors that have appreciably longer decay lengths [29] while recent findings have demonstrated that it is also important to characterize the surface sensitivity of nanoplasmonic sensors with shorter decay lengths [17,26,30]. Indeed, surface sensitivity evaluation focuses on changes in the local refractive index in close proximity to the sensor surface, which are more representative of biosensing measurements. Representative surface sensitivity evaluation approaches include atomic layer deposition of thin dielectric layers with defined thicknesses [17,31] or the adsorption of a well-defined biomacromolecular model system such as a protein monolayer [17,31] or supported lipid bilayer coating [32,33]. To date, comprehensive evaluation of bulk and surface sensitivities has been performed for various classes of laterally isotropic plasmonic nanostructures such as nanodisks and nanoholes in order to identify the best-performing ones [13,17,26,34]. However, there is still an outstanding need to systematically investigate the bulk and surface sensitivities of laterally anisotropic nanostructures such as nanorods, which can have far greater field enhancements due to high-aspect-ratio features [22,23,25,34–37] and hence could be suitable for designing high-performance nanoplasmonic sensing platforms [27,38–40].

Towards this goal, herein, we report the development of plasmonic gold nanorod (AuNR) arrays that exhibit ultrahigh surface sensitivity to detect biomacromolecular interactions with superior biosensing performance compared to other types of plasmonic nanostructures used in past studies. We employ transmission-mode LSPR sensing because it has simple instrumental requirements, high temporal resolution, and can track the real-time adsorption and conformational changes of biomacromolecules of various sizes within the sensing volume [33,41–43]. These measurement capabilities are particularly advantageous and complement other AuNR-based measurement strategies such as surface-enhanced Raman scattering (SERS) [44,45], for biointerfacial science applications, especially those involving conformational and/or shape changes that relate to the spatial proximity of adsorbed biomacromolecules. Moreover, the LSPR-based measurement readout does not rely on the density of electromagnetic hot spots and the signal response mechanism is therefore essentially independent of the orientation, arrangement, and surface coverage of AuNRs within the array. The AuNR arrays were fabricated by the colloidal deposition of short or long AuNRs on a functionalized glass substrate and initial characterization efforts focused on bulk refractive index sensitivity measurements of the AuNRs in the solution-phase and in the deposited state. The experimental results were validated by analytical calculations, which collectively provided insight into how nanorod dimensions and local dielectric environment affect plasmonic properties. Real-time biosensing experiments were also conducted to evaluate the measurement capabilities of the AuNR arrays within the context of two application examples that demand high surface sensitivity: (1) monitoring adsorption of bovine serum albumin (BSA) protein molecules, which is a widely studied biomacromolecular interaction event in the nanoplasmonic sensing field [46–48] and provided a biosensing performance benchmark; and (2) detecting peptide-induced rupture of adsorbed liposomes [32,49,50], which provided insight into tracking a complex structural transformation process.

2. Materials and methods

2.1. Reagents

Solution-phase AuNRs were obtained from nanoComposix (San Diego, CA, USA) and were classified as short (48 nm × 18 nm) or long (55 nm × 15 nm) depending on the nanostructure dimensions. The AuNRs were supplied in citrate-capped form and dispersed in deionized water. Sodium dodecyl sulfate (SDS), ethanol (99%), aminopropyltriethoxysilane (APTES, 99%), and bovine serum albumin (A2153) were purchased from Sigma-Aldrich (St. Louis, MO, USA). 1,2-dioleoyl-*sn*-glycero-3-phosphocholine (DOPC) lipids were purchased from Avanti Polar Lipids (Alabaster, AL, USA). The AH peptide used for vesicle rupture was purchased from Anaspec Corporation (San Jose, CA, USA). All aqueous solutions and buffers were prepared with Milli-Q-treated water with a minimum resistivity of 18.2 MΩ•cm (MilliporeSigma, Burlington, MA, USA). Optically polished, UV grade fused silica substrates (Corning code 7980) with 9.5 mm × 9.5 mm × 1 mm dimensions were obtained from Valley Design Corporation (Shirley, MA, USA).

2.2. UV-vis spectroscopy measurements

Plasmonic characterization of AuNRs dispersed in aqueous solution was performed by using a UV-vis spectrophotometer (UV-2700 Shimadzu, Kyoto, Japan). Solution-phase measurements were performed in absorbance mode across the 300–1000 nm wavelength range.

2.3. Bulk refractive index sensitivity measurements of AuNRs in solution

The stock AuNR solution was diluted by half in water/glycerol mixtures with increasing glycerol fraction to obtain aqueous AuNR dispersions containing 0–35% v/v glycerol in 5% increments. The extinction spectra of the AuNR dispersions were measured using the UV-vis spectrophotometer and the longitudinal peak shifts were plotted against the change in refractive index of the solution. The gradient of the plot was determined by linear regression analysis and corresponded to the bulk refractive index sensitivity of the solution-phase AuNRs.

2.4. Sensor chip fabrication

Blank glass substrates were sequentially cleaned with 1% SDS, deionized water, and ethanol, followed by drying under a stream of nitrogen gas. The substrates were then subjected to oxygen plasma treatment for 1 min prior to static incubation in a solution of 10% (v/v) APTES in ethanol for 30 min. Afterwards, the sensors were extensively washed with ethanol and dried under a stream of nitrogen gas. The APTES-coated substrates were then treated in an oven at 110 °C for 1 h, before cooling down to room temperature. Next, the APTES-coated substrates were incubated in a AuNR solution for 3 h after which they were washed with deionized water and finally dried under a stream of nitrogen gas.

2.5. Scanning electron microscopy imaging

A JEOL JSM-6700 field emission scanning electron microscope (Jeol, Tokyo, Japan) was used to characterize the surface coverage of deposited AuNRs. The AuNR-coated glass substrates were directly imaged at an accelerating voltage of 5.0 kV. Based on the images, the surface area coverage of deposited AuNRs was computed using the ImageJ software program (National Institutes of Health, Maryland, USA).

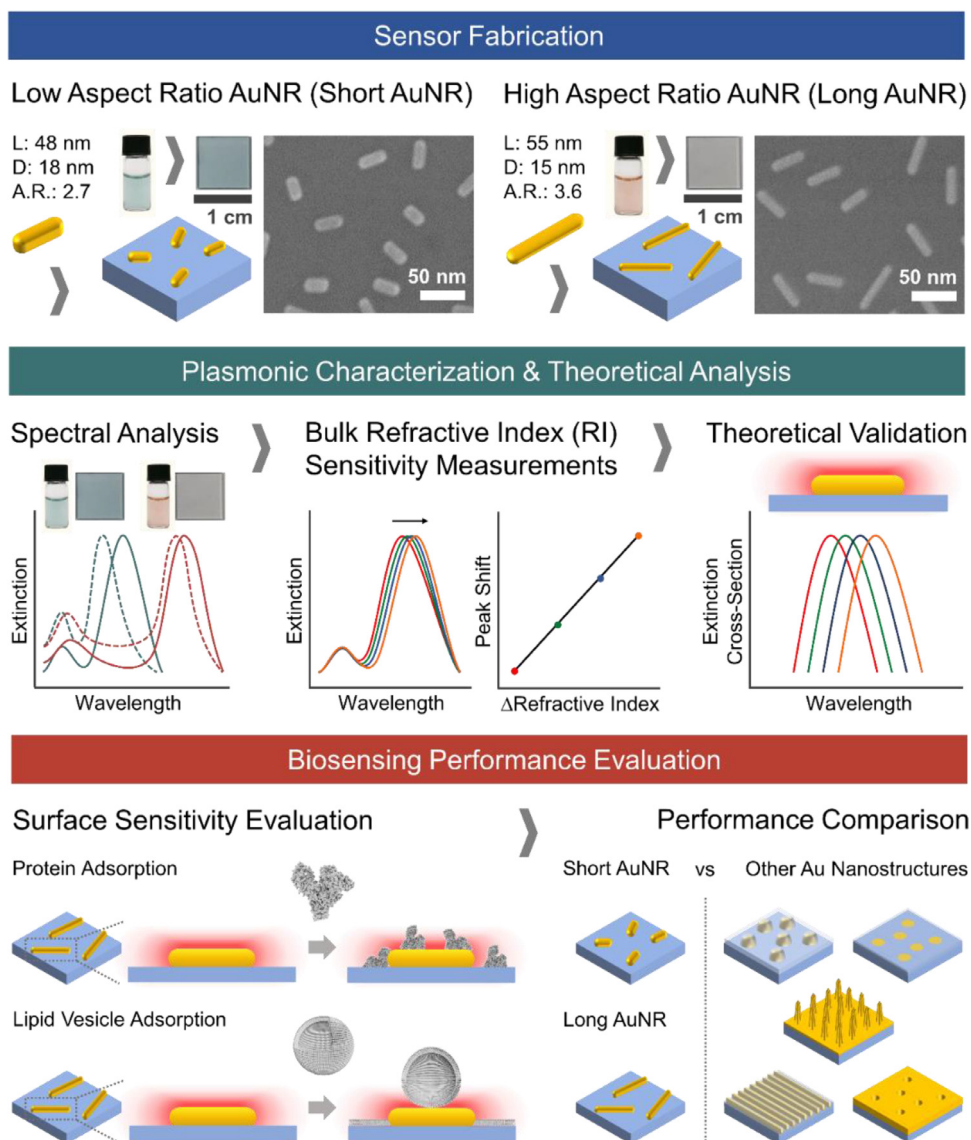


Fig. 1. Overview of experimental strategy. Top row: Sensor fabrication involved the colloidal deposition of short and long AuNRs with distinct length (L), diameter (D), and aspect ratio (A.R.) values. Photographs of the aqueous AuNR dispersions and AuNR-coated glass substrates along with scanning electron microscopy (SEM) images of the AuNR-coated glass substrates. Middle row: Plasmonic characterization of short and long AuNRs in the bulk solution and in the deposited state based on experimental measurements and analytical calculations. Bottom row: Schematic illustration of protein adsorption and vesicle-peptide interaction experiments to evaluate real-time measurement performance of the AuNR-coated glass substrates with respect to surface sensitivity, as well as biosensing performance comparison with other nanoplasmonic sensing platforms.

2.6. Localized surface plasmon resonance (LSPR) measurements

Transmission-mode LSPR experiments were conducted using an Insplorion XNano instrument (Insplorion AB, Gothenburg, Sweden). Before experiment, the as-fabricated sensor chips were subjected to oxygen plasma treatment for 30 s, before they were loaded into the microfluidic chamber. A Reglo Digital peristaltic pump (Ismatec, Glattburg, Switzerland) was used to inject liquid samples into the microfluidic chamber at a flow rate of 100 $\mu\text{L}/\text{min}$. The LSPR peak wavelength (denoted as λ_{max}) from the longitudinal plasmon mode in the optical extinction spectrum was determined by high-order polynomial fitting [51]. The measurement data were collected with a time resolution of 1 Hz, and data analysis was performed using the Insplorer software package (Insplorion AB).

2.7. Bulk refractive index sensitivity measurements of deposited AuNRs

The signal response of AuNR-coated glass substrates to different water/glycerol mixtures was measured by the LSPR technique as described above. Water/glycerol mixtures containing 0–35% v/v glycerol in 5% increments were sequentially injected into the microfluidic chamber during which shifts in the peak wavelength from the longitudinal plasmon mode in the optical extinction spectra were tracked. The longitudinal peak shifts were then plotted against the change in refractive index of the solution and the gradient of the plot was determined by linear regression analysis, which corresponded to the bulk refractive index sensitivity of deposited AuNRs.

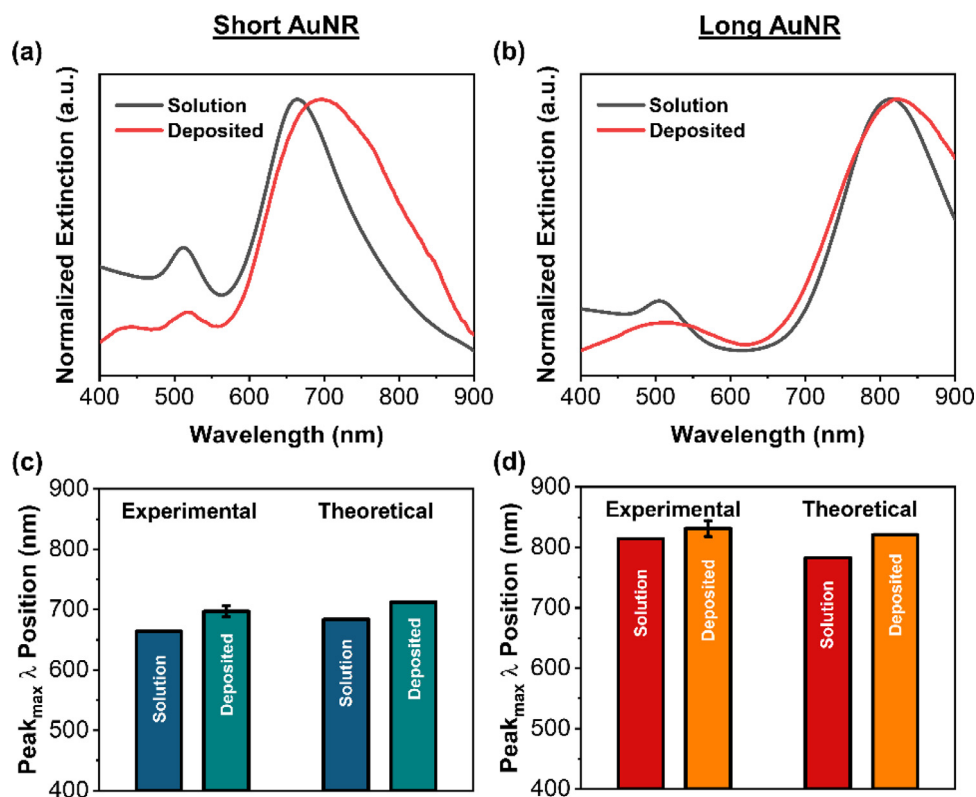


Fig. 2. Plasmonic characterization of solution-phase and deposited AuNRs. Optical extinction spectra of (a) short (low aspect ratio) and (b) long (high aspect ratio) AuNRs in bulk solution and deposited on a glass substrate. Comparison between experimentally determined and analytically calculated longitudinal λ_{max} positions for (c) short and (d) long AuNRs in bulk solution and in the deposited state. All measurements were conducted in water. Error bars represent standard deviation from $n = 3$ measurements.

3. Results and discussion

3.1. Nanoplasmonic sensing strategy

Fig. 1 presents the overall strategy to design and test a nanoplasmonic sensing platform based on plasmonically-active AuNR transducers. Two types of AuNRs with distinct aspect ratios were used: (1) low-aspect-ratio AuNRs were classified as “short” and had a typical length and diameter of 48 nm and 18 nm, respectively, and an aspect ratio of 2.7; and (2) high-aspect-ratio AuNRs were classified as “long” and had a typical length and diameter of 55 nm and 15 nm, respectively, and an aspect ratio of 3.6. The solution-phase AuNR colloids were deposited onto a glass substrate, which had been functionalized with an aminopropyltriethoxysilane (APTES) monolayer, followed by a water rinsing step. Owing to the plasmonic properties of the respective AuNRs, the glass substrates coated with short and long AuNRs exhibited uniform blue-greenish and pale purplish tints, respectively. Scanning electron microscopy (SEM) images showed that the deposited AuNRs were well-separated and had a non-periodic, non-interacting arrangement, with a low surface coverage that was equivalent to around 7–8% of the total substrate area (**Supplementary Fig. 1**).

We proceeded to experimentally characterize the plasmonic properties of the AuNR-coated glass substrates based on bulk refractive index sensitivity measurements along with theoretical analyses, and also evaluated nanoplasmonic sensing performance with respect to bulk and molecular surface sensitivities. Together, these results helped to establish the high nanoplasmonic sensing performance of the AuNR-coated glass substrates and to place these performance capabilities within the context of broader developments in the nanoplasmonic biosensing field as a whole.

3.2. Plasmonic characterization

Transmission-mode UV–vis spectroscopy experiments were initially conducted to characterize the ensemble-average plasmonic properties of the short and long AuNRs in bulk solution and in the deposited state. In all cases, the optical extinction spectra were measured and the AuNRs exhibited LSPR behavior, as indicated by two peaks in the extinction spectra that corresponded to the transverse and longitudinal plasmon modes, respectively (**Figs. 2a,b**). For both AuNRs, there was more intense extinction at the longitudinal peak and the specific λ_{max} position of the longitudinal peak depended on the local dielectric environment, *i.e.*, suspended in the solution phase or deposited on the glass substrate. Hence, the λ_{max} position of the longitudinal peak was the main focus of our experimental testing and theoretical analyses.

Fig. 2c presents the experimentally determined longitudinal λ_{max} positions for short AuNRs and the peak shifted from ~665 nm in bulk solution to ~680 nm in the deposited state. This measurement result agreed well with the trend predicted by theoretical extinction cross-section calculations, which determined the longitudinal λ_{max} position by modeling the single AuNR as a prolate spheroid with spherical cylinder geometry and describing the Drude-Lorentz model (see Supplementary Information for more details) [52]. Indeed, the theoretically calculated longitudinal λ_{max} positions for short AuNRs were ~683 nm and ~710 nm in bulk solution and in the deposited state, respectively.

A similar trend in longitudinal λ_{max} positions was also observed for long AuNRs (**Fig. 2d**). The experimentally determined longitudinal λ_{max} position shifted from ~814 nm in bulk solution to ~831 nm in the deposited state. Likewise, the theoretically calculated longitudinal λ_{max} positions for long AuNRs were ~780 nm

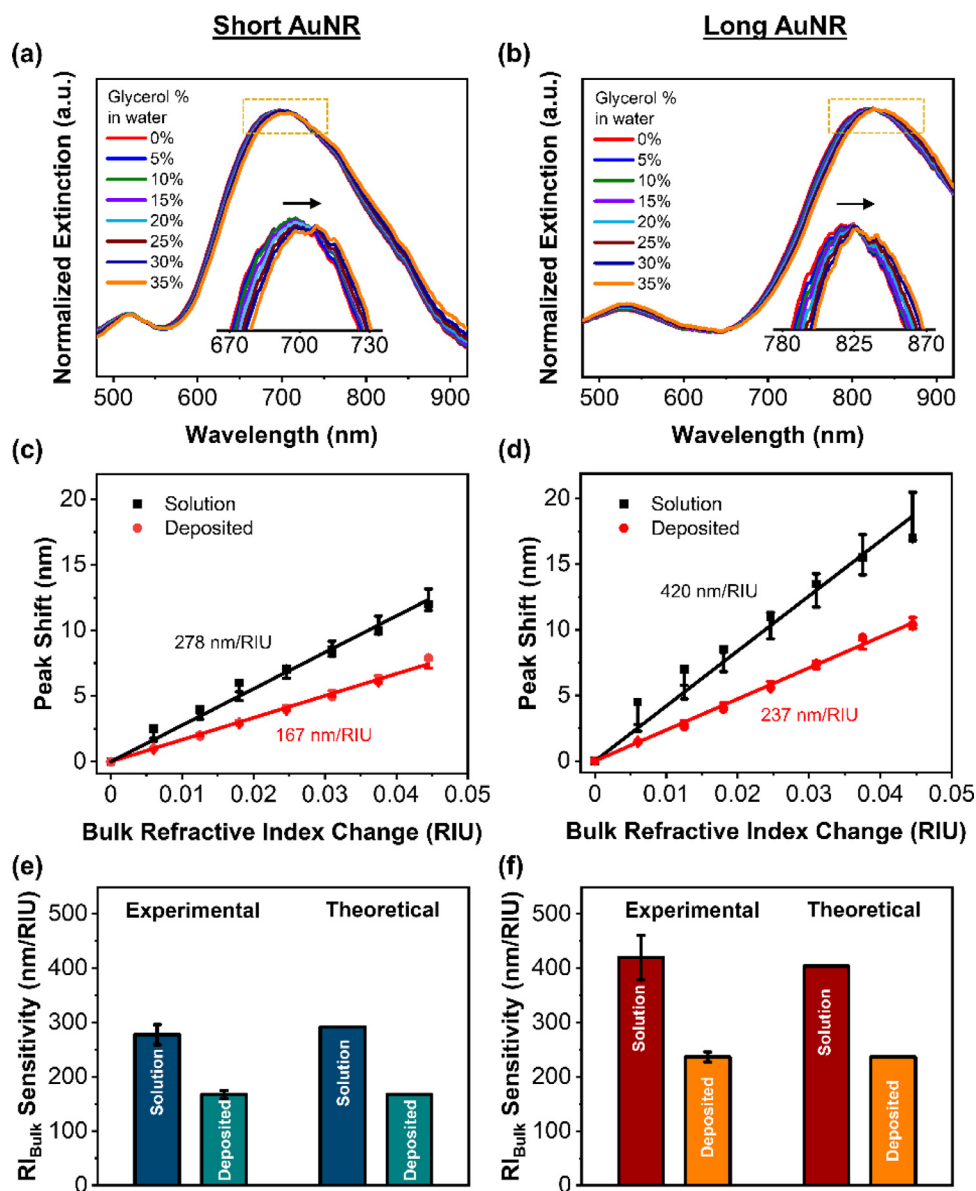


Fig. 3. Bulk refractive index sensitivities of solution-phase and deposited AuNRs. Optical extinction spectra of deposited (a) short and (b) long AuNRs in the presence of different water/glycerol mixtures (0–35% v/v glycerol). Experimentally measured bulk refractive index sensitivities of solution-phase and deposited (c) short and (d) long AuNRs based on the longitudinal $\Delta\lambda_{\max}$ shift responses in water/glycerol mixtures with different refractive index values. The lines are linear best-fits of the measurement data and the reported bulk refractive index sensitivity values are reported from the corresponding slopes. Comparison between experimentally determined and analytically calculated bulk refractive index sensitivities of (e) short and (f) long AuNRs in bulk solution and in the deposited state. Data are reported as mean \pm standard deviation from $n = 3$ measurements.

and ~ 820 nm in bulk solution and in the deposited state, respectively. Together, the experimental data and theoretical analyses support that the longitudinal λ_{\max} position of AuNRs is sensitive to the change in local dielectric environment that is associated with colloidal deposition. Since a large fraction of the AuNR surface comes into close contact with the glass substrate, the corresponding effect on plasmonic properties is appreciable compared to the colloidal deposition of other types of nanostructures such as spherical Au nanoparticles, in which case there is a smaller contact area and accordingly a nearly negligible shift in the λ_{\max} position of its single LSPR extinction peak (Supplementary Fig. 2).

3.3. Bulk sensitivity measurements

The bulk refractive index sensitivities of the short and long AuNRs in bulk solution and in the deposited state were also ex-

perimentally characterized by measuring the corresponding longitudinal $\Delta\lambda_{\max}$ shifts in different water-glycerol mixtures (0–35% v/v glycerol, in 5% increments) (Figs. 3a,b and Fig. S3). In general, the longitudinal $\Delta\lambda_{\max}$ position increased at higher glycerol fractions, indicating a sensitive response to changes in bulk refractive index within the tested range.

For short AuNRs, plots of the $\Delta\lambda_{\max}$ shift as a function of the change in bulk refractive index units (Δ RIU) showed linear trends and the corresponding bulk refractive index sensitivities were 277.5 and 167.3 nm/RIU for short AuNRs in bulk solution and in the deposited state, respectively (Fig. 3c). The diminished bulk sensitivity of the short AuNRs on the glass substrate likely originates from the large degree of contact area with the substrate since the contacting region of the nanostructure is no longer sensitive to changes in the bulk environment [35,53]. Likewise, for long AuNRs, the plots showed linear responses and the corresponding

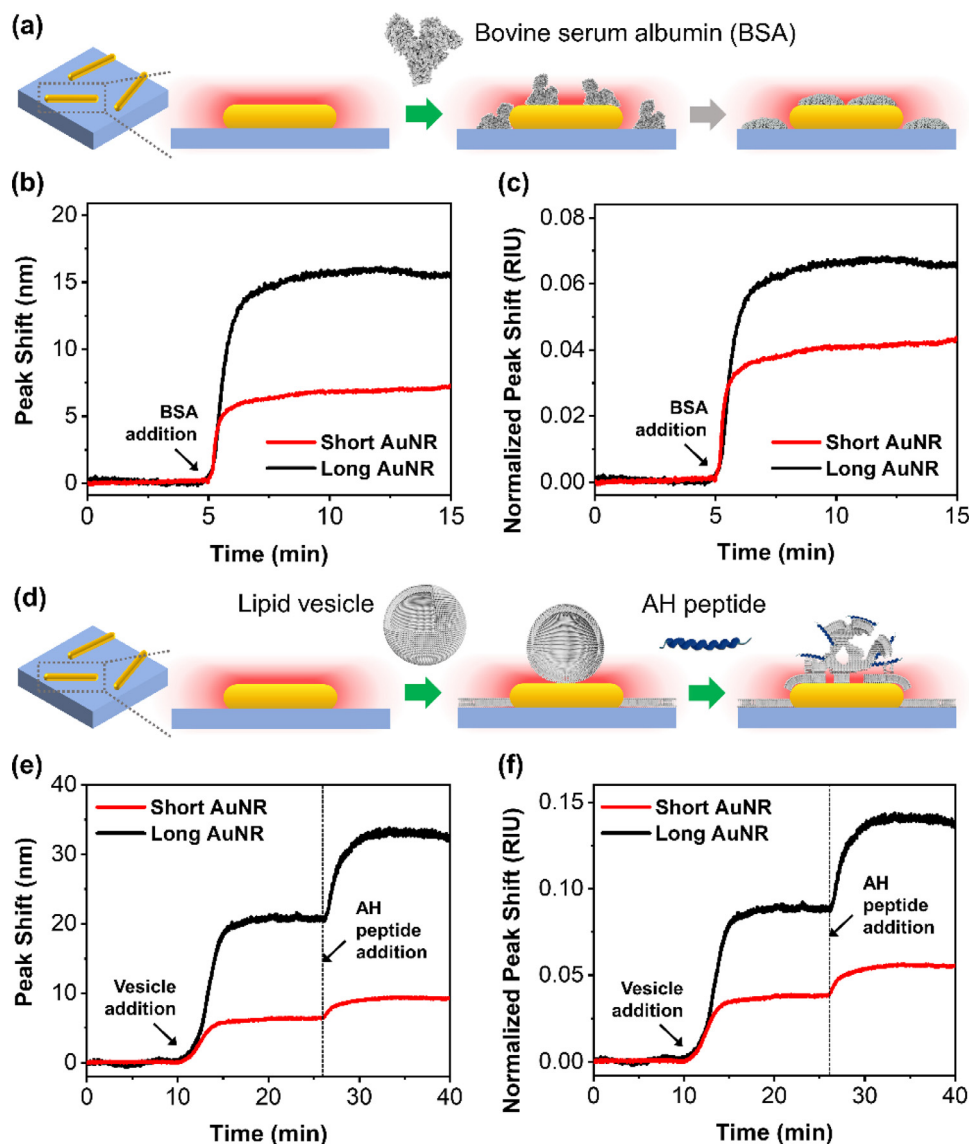


Fig. 4. Real-time biosensing experiments to evaluate the measurement performance of deposited AuNR arrays with respect to surface sensitivity. (a) Schematic illustration of bovine serum albumin (BSA) protein adsorption onto AuNR-coated glass substrates. (b) Time-resolved $\Delta\lambda_{\max}$ shifts and corresponding (c) time-resolved Δ RIU shifts for tracking BSA protein adsorption onto short and long AuNR-coated glass substrates. The baseline signals were recorded in aqueous buffer solution before BSA protein was added at $t = 5$ min. (d) Schematic illustration of DOPC lipid vesicle adsorption onto AuNR-coated glass substrates, followed by AH peptide-induced vesicle rupture. (e) Time-resolved $\Delta\lambda_{\max}$ shifts and corresponding (f) time-resolved Δ RIU shifts for tracking DOPC lipid vesicle adsorption, followed by AH peptide addition to rupture adsorbed vesicles on short and long AuNR-coated glass substrates. The baseline signals were recorded in aqueous buffer solution before DOPC lipid vesicles and AH peptide were added at $t = 10$ and $t = 25$ min, respectively.

bulk refractive index sensitivities were 419.5 and 236.6 nm/RIU for long AuNRs in bulk solution and in the deposited state, respectively (Fig. 3d). The latter value is comparable to the bulk refractive index sensitivity of ~ 100 -nm diameter Au nanodisks on a glass substrate.

The experimental results were confirmed by analytical calculations, which agreed well in terms of the absolute bulk refractive index sensitivity values and further support that the $\sim 40\%$ decrease in bulk refractive index sensitivity for deposited AuNRs is due to contact with the glass substrate (Figs. 3e,f and Supplementary Fig. 4; see Supplementary data for more details). Notably, the bulk refractive index sensitivities for short and long AuNRs were appreciably higher than the values recorded for suspended and deposited, spherical Au nanoparticles, which were around 68.2 and 58.7 nm/RIU, respectively (Supplementary Fig. 5). Collectively, these findings indicate the high bulk refractive index sensitivities of the AuNR-coated glass substrates and led us to further investi-

gate the surface sensitivities in response to biosensing events that occur near the sensor surface.

3.4. Surface sensitivity evaluation

We conducted a series of liquid-phase biosensing experiments with AuNR-coated glass substrates that were enclosed in a flow-through microfluidic chamber. In the first experimental set, we measured the real-time adsorption of 100 μ M bovine serum albumin (BSA) protein onto the AuNR-coated glass substrates, which is a widely used biosensing measurement to evaluate surface sensitivity (Fig. 4a). Rapid increases in the $\Delta\lambda_{\max}$ signals indicated monotonic adsorption until there was saturation of adsorbed protein molecules within a well-packed monolayer [46,48] (Fig. 4b). The corresponding $\Delta\lambda_{\max}$ shifts at saturation were around 6 and 16 nm for short and long AuNRs, respectively, which are much higher values than typically observed for BSA adsorption onto

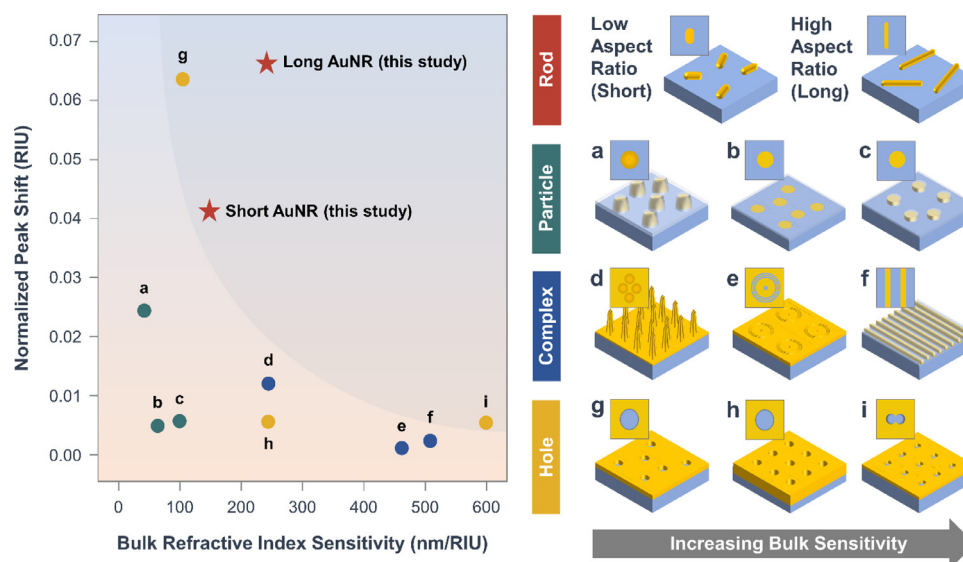


Fig. 5. Biosensing performance comparison of deposited AuNR arrays with other classes of plasmonic nanostructures reported in the literature. A plot of normalized Δ RIU shift in response to BSA protein adsorption vs. bulk refractive index sensitivity is presented for different nanoplasmonic sensing platforms based on nanorods, nanoparticles, complex nanostructures, and nanoholes. Each symbol represents a single type of nanoplasmonic sensing platform and schematic illustrations of the different platforms are presented, which are coded by letter and were reported in the following references: a-[54], b-[55], c-[56], d-[57], e-[31], f-[58], g-[59], h-[60], i-[61].

other types of nanoplasmonic sensor surfaces with similar bulk sensitivities. To directly compare the measurements results across the two AuNR-coated glass substrates, we converted the $\Delta\lambda_{\max}$ shifts into corresponding Δ RIU shifts by taking into account the bulk refractive index sensitivity of each sensor surface and the corresponding Δ RIU shifts at saturation were around 0.04 and 0.06 RIU for short and long AuNRs, respectively (Fig. 4c).

We next investigated real-time biosensing capabilities to detect the transformation of intact, adsorbed vesicles into a supported lipid bilayer (SLB) coating upon addition of a membrane-rupturing, amphipathic α -helical (AH) peptide [32] (Fig. 4d). This multi-step process first involved the adsorption of lipid vesicles onto the AuNR-coated glass substrates, which resulted in corresponding $\Delta\lambda_{\max}$ shifts of around 6 and 18 nm for short and long AuNRs, respectively (Fig. 4e). The addition of 13 μ M AH peptide to the adsorbed vesicles then triggered vesicle rupture, which resulted in lipid reorganization and SLB formation that yielded final $\Delta\lambda_{\max}$ shifts of around 8 and 32 nm for short and long AuNRs, respectively. These responses are significantly larger than the responses observed due to AH peptide-mediated rupture of adsorbed vesicles on other nanoplasmonic sensing platforms [32], which is in line with the BSA adsorption results. Further investigation of the corresponding Δ RIU shifts that the long AuNRs had greater than two-fold improved sensing performance over the short AuNRs (Fig. 4f).

3.5. Biosensing performance comparison

There is extensive interest in defining performance metrics for nanoplasmonic biosensors and one of the most widely used metrics is the bulk refractive index sensitivity value. In general, a larger bulk sensitivity value is considered an indicator of better sensing performance and is associated with a larger probing volume, *i.e.*, the decay length of the LSPR-enhanced electromagnetic field is greater. On the other hand, most biosensing measurements demand high surface sensitivity, which corresponds to a large plasmonic signal in response to a change in the local refractive index near the sensor surface. Surface sensitivity is often associated with a low probing volume and hence it is important to consider both bulk sensitivity and surface sensitivity when evaluating sens-

ing performance [12,17,30]. Furthermore, as mentioned above, a commonly used method to assess surface sensitivity is to measure the change in plasmonic signal that is associated with BSA protein adsorption onto a sensor surface.

To contextualize the sensing performance of the AuNR-coated glass substrates, we plotted a graph that summarizes the normalized Δ RIU shifts for BSA adsorption vs. bulk refractive index sensitivity for various types of Au nanoplasmonic sensing platforms that have been reported in the scientific literature (Fig. 5).

For most nanostructures, the Δ RIU shift for BSA adsorption was less than 0.02 across a wide range of bulk refractive index sensitivity values ranging from around 50 to 600 nm/RIU. This finding reinforces that the surface and bulk sensitivities of a sensing platform are distinct performance metrics. In fact, a nanodisk platform with a low bulk refractive index sensitivity of 40 nm/RIU yielded a relatively high Δ RIU shift of 0.023 for BSA adsorption [54]. Moreover, there were only three nanoplasmonic sensing platforms that yielded Δ RIU shifts of greater than 0.04, including the two AuNR arrays in this work and a nanohole array [59]. Notably, the long AuNR array in this study had the highest surface sensitivity with a Δ RIU shift of 0.066 for BSA adsorption, which is also an order of magnitude higher than typical responses from traditional SPR (Δ RIU shifts of \sim 0.001) [62–64] and nanoparticle-enhanced SPR (Δ RIU shifts of \sim 0.004) [65] sensing platforms that were operated in the attenuated total reflection (ATR) configuration. Such improvement is likely enabled by the significant electromagnetic field enhancement surrounding the edges of high-aspect-ratio nanostructures. Other key factors contributing to the ultrahigh surface sensitivity include the tightly confined field enhancement (short decay length) for AuNRs in the tested size range [66] along with the absence of a surfactant layer on the AuNR surface due to the oxygen plasma pretreatment [67–69].

In addition to the physical dimensions of the AuNRs, the resultant biosensing performance also depends on the dimensions of the target biomacromolecules relative to the region of tightly confined field enhancement (*i.e.*, effective sensing volume of the AuNRs) [17,30,70]. In this case, a close match between the size of BSA molecules (*i.e.*, \sim 14 nm x 4 nm x 4 nm) [71] and the field decay length (*i.e.*, \sim 5–20 nm) [17,18] suggests that a significant portion of the biomacromolecule is found within the sensing volume.

It should also be pointed out that, since the measurements have an ensemble-averaged readout, the overall measurement signal is essentially a collective representation of the signals from individual AuNRs [72,73]. The sensing performance of a single AuNR can theoretically be improved down to single-molecule detection by tuning the geometry of the AuNR in relation to the dimensions of the target molecule, regardless of the arrangement of the AuNRs within the array and/or the array dimensions [74–78]. This is a notable potential advantage compared to other modes of plasmonic sensing such as SERS [44,45], Fano resonance [79–81], extraordinary transmission (EOT) [82,83], and plasmon-coupled whispering gallery mode (WGM) [84–86], in which cases an ordered arrangement of nanoplasmonic transducers is often an essential feature for sensing and additional considerations need to be carefully made with respect to the order and periodicity of the nanoplasmonic transducers as well as the array dimensions—all of which influence sensing performance.

4. Conclusions

Growing attention to the importance of surface sensitivity as a nanoplasmonic biosensing performance metric has led to the exploration of a wide range of nanostructure shapes and sizes in order to finetune plasmonic features such as the field decay length. To date, most related efforts have focused on laterally isotropic nanostructures (e.g., circular nanodisks and nanoholes), while our findings demonstrate the sensing merits of utilizing laterally anisotropic nanostructures (e.g., nanorods). Indeed, the experimental results in this work revealed that the high-aspect-ratio AuNR arrays had superior biosensing performance to detect adsorbed BSA protein molecules as compared to a wide range of other plasmonic nanostructures tested in past studies. These results motivate the continued exploration of laterally anisotropic nanostructures as plasmonic transducers, especially in combination with broadly applicable colloidal deposition strategies (as opposed to more complex fabrication techniques) and with due consideration of how tuning the nanostructure geometry can yield larger field enhancement effects and shorter decay lengths. It is the combination of these two factors – a large field enhancement and short decay length – that contributes to the high surface sensitivity, which is advantageous for biosensing. From a broader perspective, our findings also emphasize that surface sensitivity is a critical performance metric over bulk sensitivity in order to guide the design of high-performance nanoplasmonic sensors for biosensing applications.

Declaration of competing interest

The authors declare that they have no known competing financial interests or personal relationships that could have appeared to influence the work reported in this paper.

Credit authorship contribution statement

Abdul Rahim Ferhan: Conceptualization, Investigation, Writing - original draft, Writing - review & editing. **Youngkyu Hwang:** Investigation, Writing - review & editing. **Mohammed Shahrudin Bin Ibrahim:** Investigation, Writing - review & editing. **Shikhar Anand:** Methodology, Formal analysis, Writing - review & editing. **Ahram Kim:** Methodology, Formal analysis, Writing - review & editing. **Joshua A. Jackman:** Conceptualization, Writing - original draft, Writing - review & editing, Supervision. **Nam-Joon Cho:** Conceptualization, Writing - review & editing, Supervision.

Acknowledgments

This work was supported by the National Research Foundation of Korea (NRF) grant funded by the Korean government (MSIT) (No.

2020R1C1C1004385), by the SKKU Research Fellowship Program of Sungkyunkwan University, and by the MOTIE (Ministry of Trade, Industry, and Energy) in Korea, under the Fostering Global Talents for Innovative Growth Program (P0008746) supervised by the Korea Institute for Advancement of Technology (KIAT). In addition, this work was partially supported by the Starting Growth Technological R&D program of SMBA (S2850950).

Data availability

The raw data required to reproduce these findings are available from the corresponding authors on reasonable request.

Supplementary materials

Supplementary material associated with this article can be found, in the online version, at [doi:10.1016/j.apmt.2021.101046](https://doi.org/10.1016/j.apmt.2021.101046).

References

- [1] M.I. Stockman, *Science* 348 (6232) (2015) 287.
- [2] A.G. Brolo, *Nat Photonics* 6 (11) (2012) 709.
- [3] J.N. Anker, et al., *Nat Mater* 7 (6) (2008) 442.
- [4] A.B. Dahlin, et al., *Nanophotonics* 2 (2) (2013) 83.
- [5] O. Tokel, *Chem. Rev.* 114 (11) (2014) 5728.
- [6] A.R. Ferhan, *Nanoscale Advances* 2 (8) (2020) 3103.
- [7] J.A. Jackman, *Bull. Chem. Soc. Jpn.* 92 (8) (2019) 1404.
- [8] J.A. Jackman, *Chem Soc Rev* 46 (12) (2017) 3615.
- [9] K. Ariga, *Adv Funct Mater* 28 (27) (2018) 1702905.
- [10] E. Mauriz, *Analyst* 144 (24) (2019) 7105.
- [11] G.A. Lopez, *Nanophotonics* 6 (1) (2017) 123.
- [12] S.-H. Oh, H. Altug, *Nat Commun* 9 (1) (2018) 5263.
- [13] M. Vala, *ACS Sensors* 4 (12) (2019) 3265.
- [14] B. Doiron, *ACS Photonics* 6 (2) (2019) 240.
- [15] K.A. Willets, R.P. Van Duyne, *Annu Rev Phys Chem* 58 (1) (2007) 267.
- [16] Y. Jeong, *Biosens Bioelectron* 111 (2018) 102.
- [17] F. Mazzotta, *ACS Photonics* 2 (2) (2015) 256.
- [18] H. Im, *ACS Nano* 4 (2) (2010) 947.
- [19] H. Xin, *Nat Rev Mater* 3 (8) (2018) 228.
- [20] L. Guo, *Nano Today* 10 (2) (2015) 213.
- [21] S. Unser, *Sensors* 15 (7) (2015) 15684.
- [22] B. Špačková, *ACS Photonics* 5 (3) (2018) 1019.
- [23] C. Du, *PCCP* 21 (14) (2019) 7654.
- [24] B. Špačková, *Proc IEEE* 104 (12) (2016) 2380.
- [25] G.K. Joshi, *The Journal of Physical Chemistry C* 116 (39) (2012) 20990.
- [26] J. Li, *The Journal of Physical Chemistry C* 119 (52) (2015) 29116.
- [27] T. Xu, Z. Geng, *Biosens Bioelectron* 174 (2021) 112850.
- [28] S. Szunerits, R. Boukherroub, *Chem Commun* 48 (72) (2012) 8999.
- [29] J. Homola, *Chem. Rev.* 108 (2) (2008) 462.
- [30] J. Li, *ACS Photonics* 2 (3) (2015) 425.
- [31] B. Zeng, *Nanoscale* 7 (1) (2015) 166.
- [32] G.H. Zan, *Small* 10 (23) (2014) 4828.
- [33] A.R. Ferhan, *Anal. Chem.* 90 (21) (2018) 12503.
- [34] L. Yang, *Chem Soc Rev* 48 (19) (2019) 5140.
- [35] O. Saison-Francioso, *The Journal of Physical Chemistry C* 119 (51) (2015) 28551.
- [36] S. Link, M.A. El-Sayed, *J Phys Chem B* 109 (20) (2005) 10531.
- [37] S. Link, M.A. El-Sayed, *Int Rev Phys Chem* 19 (3) (2000) 409.
- [38] H. Chen, *Chem Soc Rev* 42 (7) (2013) 2679.
- [39] L. Vigderman, *Adv Mater* 24 (36) (2012) 4811.
- [40] J.-E. Park, *ACS Cent Sci* 4 (10) (2018) 1303.
- [41] C. Langhammer, *Nano Lett.* 10 (9) (2010) 3529.
- [42] A.R. Ferhan, *Anal. Chem.* 89 (7) (2017) 4301.
- [43] F.A.A. Nugroho, *ACS Nano* 14 (2) (2020) 2345.
- [44] J. Langer, *ACS Nano* 14 (1) (2020) 28.
- [45] N.S. Mueller, *ACS Nano* 15 (3) (2021) 5523.
- [46] G.J. Ma, *Communications Materials* 1 (1) (2020) 45.
- [47] A.R. Ferhan, *Sensors* 18 (4) (2018).
- [48] J.H. Park, *PCCP* 19 (13) (2017) 8854.
- [49] A.R. Ferhan, *Anal. Chem.* 88 (24) (2016) 12524.
- [50] N.-J. Cho, *Anal. Chem.* 81 (12) (2009) 4752.
- [51] A.B. Dahlin, *Anal. Chem.* 78 (13) (2006) 4416.
- [52] M.D. Thoreson, *Sandia Report* (2010) **SAND2009-7034**.
- [53] C. Novo, *The Journal of Physical Chemistry C* 112 (1) (2008) 3.
- [54] R. Frost, *Nanoscale* 9 (10) (2017) 3620.
- [55] F.A.A. Nugroho, *ACS Sensors* 2 (1) (2017) 119.
- [56] J.A. Jackman, *Anal. Chem.* 89 (23) (2017) 12976.
- [57] D. Pallarola, *Chem Commun* 49 (75) (2013) 8326.
- [58] C. Zhao, *Nano Lett.* 20 (3) (2020) 1747.
- [59] D. Gao, *Appl Phys Lett* 90 (7) (2007) 073901.
- [60] A. Hsiao, *Sens Biosensing Res* 5 (2015) 24.
- [61] A. Lesuffleur, *Appl Phys Lett* 90 (24) (2007) 243110.

- [62] G.B. Sigal, *J. Am. Chem. Soc.* 120 (14) (1998) 3464.
- [63] R.J. Green, *Biomaterials* 20 (4) (1999) 385.
- [64] V. Silin, *J Colloid Interface Sci* 185 (1) (1997) 94.
- [65] E.M.S. Azzam, *Thin Solid Films* 518 (1) (2009) 387.
- [66] L. Tian, *Langmuir* 28 (50) (2012) 17435.
- [67] E. Martinsson, *Small* 12 (3) (2016) 330.
- [68] D. Jana, *Anal. Chem.* 87 (7) (2015) 3964.
- [69] J. He, *Colloids Surf B Biointerfaces* 163 (2018) 140.
- [70] O. Kedem, *ACS Nano* 5 (2) (2011) 748.
- [71] T. Peters, 3 - Serum Albumin, in: F.W. Putnam (Ed.), *The Plasma Proteins, Second Edition*, Academic Press, 1975, p. 133.
- [72] C. Tserkezis, *Sci Rep* 6 (1) (2016) 28441.
- [73] A.B. Dahlin, *Sensors* 12 (3) (2012).
- [74] Z. Omair, M.A. Talukder, *Plasmonics* 14 (6) (2019) 1611.
- [75] M.A. Beuwer, *Nano Lett.* 15 (5) (2015) 3507.
- [76] G.J. Nusz, *Anal. Chem.* 80 (4) (2008) 984.
- [77] G.J. Nusz, *ACS Nano* 3 (4) (2009) 795.
- [78] R.E. Armstrong, *Small* 16 (52) (2020) 2003934.
- [79] Z. Liu, J. Ye, *Nanoscale* 8 (40) (2016) 17665.
- [80] B. Luk'yanchuk, *Nat Mater* 9 (9) (2010) 707.
- [81] Y. Francescato, *ACS Nano* 6 (2) (2012) 1830.
- [82] S.G. Rodrigo, *Proc IEEE* 104 (12) (2016) 2288.
- [83] S. Tajik, Z. Atlasbaf, *J Appl Phys* 127 (2) (2020) 023102.
- [84] W. Liu, *Nano Lett.* 21 (4) (2021) 1566.
- [85] S. Frustaci, F. Vollmer, *Curr Opin Chem Biol* 51 (2019) 66.
- [86] N. Toropov, *Light: Science & Applications* 10 (1) (2021) 42.